Characterization of the interface properties in a-Si:H/c-Si heterostructures by photoluminescence

S Tardon, R Brüggemann

Characterisation of the interface properties in a-Si:H/c-Si heterostructures by photoluminescence

S.Tardon, R. Brüggemann[1]

Institut für Physik, Carl von Ossietzky Universität Oldenburg, D-26111 Oldenburg, Germany

ABSTRACT: Photoluminescence measurements on hydrogenated amorphous silicon / crystalline silicon (a-Si:H / c-Si) heterostructures have been used for two aspects of their characterisation: the monitoring of the crystalline silicon wafers and of their interface properties after different steps of solar cell processing and the tracking of interface properties on purpose-built symmetrical structures with different amorphous silicon overlayers. The difference in the quasi-Fermi level splittings in these symmetrical structures, determined both experimentally and by numerical modelling, suggest an energetic position of the interface defect distribution with a peak at around 0.7 eV – 0.8 eV above the c-Si valence band edge. Numerical modelling is also applied to the structures after solar-cell processing steps and consistently tracks the variation in quasi-Fermi level splitting, i.e., excess carrier densities, in the c-Si layer. The agreement in the experimental and simulated open-circuit voltages for the final cell adds confidence to the interface defect parameters determined.

PACS: 78.55.-m, 72.20.Jv, 73.20.-r, 88.40.H-,

Keywords: photoluminescence, recombination, a-Si:H/c-Si, heterostructure, solar cell

[1] Corresponding author, email rudi.brueggemann@uni-oldenburg.de

1. Introduction

Heterojunction solar cells based on hydrogenated amorphous silicon (a-Si:H) layers on crystalline silicon (c-Si) wafers have been developed over the last twenty years [1] and efficiencies in excess of 20% have been achieved [2]. A prerequisite to a high efficiency a-Si:H/c-Si heterojunction is a high quality amorphous/crystalline interface, as otherwise the solar cell properties are limited by recombination at the a-Si:H/c-Si interface [2-7]. Characterisation techniques, such as photoluminesence (PL) measurements, may be applied to study the influence of the interface defects on the minority carrier density in the volume of the cell [6,7].

The description of the photoluminescence (PL) radiation emitted from a semiconductor by Planck's generalised law [8,9] gives access to the splitting of the quasi-Fermi levels ($E_{Fn} - E_{Fp}$), where E_{Fn} and E_{Fp} are the electron and hole quasi-Fermi levels that describe the densities of free electrons and holes in the conduction and valence band, respectively. The energetic separation of the Fermi energies, (E_{Fn}–E_{Fp}), in the volume of a wafer or solar cell is reduced via non-radiative transitions, such as bulk or surface/interface recombination via defects. The influence of surface recombination is noticeable in typical crystalline silicon (c-Si) solar cells, especially if the minority-carrier diffusion lengths are longer than the absorber thicknesses. It is thus possible to take the volume radiation recombination rate monitored by the PL measurement as an indicator of the interface quality that is of interest in a-Si:H/c-Si structures. Thus, we have applied such PL measurements for the characterisation of the interfaces for different wafer cleaning schemes and a-Si:H passivation layers [7]. The PL technique can also be applied to "precursor" structures after the different steps of solar cell processing, respectively, as has been shown on chalcopyrite cell structures [10]. These measurements have a strong relevance to the optimisation of solar cell performance since the magnitude of the quasi-Fermi level splitting gives an indication of the achievable open circuit voltage V_{OC} in a final device [9].

Two aspects concerning the exploitation of PL measurements are dealt with in this paper: i) We analyse different steps in a standard production process of a-Si:H/c-Si solar cells with final AM1.5-efficiencies > 14 % via quantitative photoluminescence measurements. ii) We apply PL measurements to obtain information on the interface defect distribution by studying p-type c-Si wafers in which the Fermi level positions at the amorphous / crystalline interface are adjusted by a variation in a-Si:H layer sequences. Numerical modelling assists in the interpretation of the results.

2. Theoretical Background

The spectrally dependent absorptivity $A(\hbar\omega)$ of a material slab can be calculated as

$$A(\hbar\omega) = \frac{(1-R_F(\hbar\omega))(1+R_B(\hbar\omega)\mathrm{e}^{-\alpha(\hbar\omega)d})(1-\mathrm{e}^{-\alpha(\hbar\omega)d})}{1-R_F(\hbar\omega)\mathrm{R}_B(\hbar\omega)\mathrm{e}^{-2\alpha(\hbar\omega)d}} \tag{1}$$

where $R_F(\hbar\omega)$ and $R_B(\hbar\omega)$ are the reflection coefficients at the front and back surface of the semiconductor, $\alpha(\hbar\omega)$ is the absorption coefficient, and d is the thickness of the slab. For $R_F = R_B$, Eq. (1) corresponds with Eq. (24) of [8].

Assuming that the carrier distributions of electrons and holes, n and p, can be described by quasi-Fermi level statistics and that the quasi-Fermi level splitting for electrons and holes, $\Delta E_F = E_{Fn} - E_{Fp}$, is independent of position, the photoluminescent photon flux $\mathrm{d}j_\gamma$, emitted from a semiconductor surface in an energy interval $\mathrm{d}(\hbar\omega)$ into one hemisphere is described by a generalised Kirchhoff law given by [8,9]

$$\mathrm{d}j_\gamma = \frac{A(\hbar\omega)}{4\pi^2\hbar^3\mathrm{c}^2}\frac{(\hbar\omega)^2\mathrm{d}(\hbar\omega)}{\exp\left[\dfrac{\hbar\omega-(E_{Fn}-E_{Fp})}{kT}\right]-1} \tag{2}$$

where k is the Boltzmann constant and c is the speed of light in vacuum. The absorptivity/emissivity term $A(\hbar\omega)$ is that of Eq. (1).

Under typical excitation conditions, Eq. (2) reduces to

$$\mathrm{d}j_\gamma = \frac{A(\hbar\omega)}{4\pi^2\hbar^3\mathrm{c}^2}(\hbar\omega)^2\exp\left(-\frac{\hbar\omega}{kT}\right)\exp\left(\frac{E_{Fn}-E_{Fp}}{kT}\right)\mathrm{d}(\hbar\omega)\cdot \tag{3}$$

The exponential term with $E_{Fn} - E_{Fp}$ reflects the product np/n_i^2 for radiative recombination which shifts the spectral distribution without changing its shape, provided that $E_{Fn} - E_{Fp}$ is spatially constant.

3. Experimental Details

The photoluminescence radiation was measured using a lock-in technique at room temperature using a laser diode with a wavelength $\lambda = 782$ nm as an excitation source, with a photon flux of 1.6×10^{18} photons cm^{-2} s^{-1} (~ 4 × AM1.5). The photoluminescence was detected by a LN_2-cooled InGaAs detector positioned at the exit slit of a 0.25 m grating monochromator.

The calibration of the setup was performed using a tungsten filament lamp source placed at the sample position, allowing a quantitative measurement of the emitted photon flux in the photoluminescence experiment, and therefore the determination of the quasi-Fermi level splitting according to Eq. (2).

The samples were deposited at the Institut für Physikalische Elektronik in Stuttgart. Figure 1 sketches the sample series which was deposited on a double-sided polished p-type c-Si wafer (thickness 250 µm and 0.8-1 Ωcm). It includes a symmetrical (i)a-Si:H/(p)c-Si/(i)a-Si:H structure (figure 1a) passivated with two 8 nm thin intrinsic a-Si:H layers and an (n)a-Si:H/(i)a-Si:H/(p)c-Si/(i)a-Si:H/(n)a-Si:H (figure 1b) structure. Technically, the structure of figure 1a received the additional n-layers so that the (i)a-Si:H/(p)c-Si interfaces are the same. These samples were designed in order to obtain symmetrical optical and structural properties at the back and front of the wafer with different Fermi levels at the interfaces. Figure 1c shows the precursor of the solar cell with different doped a-Si:H layers with an (n)a-Si:H/(i)a-Si:H/(p)c-Si/(i)a-Si:H/(p)a-Si:H sequence. Figure 1d shows the complete cell with the constituent layers deposited on the same remaining pieces of the wafer after respective surface cleaning and pre-treatment. Following these procedures, all pieces of the original wafer should have identical properties of the (p)c-Si/(i)a-Si:H interface.

4. Numerical modelling

Numerical modelling has been applied with the device modelling program SC-Simul [11,12]. It solves the full set of device and transport equations and has been successfully applied to a-Si:H/c-Si heterostructures [13,14]. For the purpose of extracting information on the interface defect distribution we have simulated photoluminescence for each of the previously described types of samples and determined the electron and hole distributions from which $E_{Fn} - E_{Fp}$ was calculated.

The defects at the interface N_{if} were represented by a Gaussian profile of energetic width σ and peak energy $E_{p,}$ both of which are varied in the simulation study. The nature of the interface defect was taken as that of a dangling bond with its three possible charge states and corresponding densities of positive (D+), neutral (D0) and negative (D–) defects. The statistics in terms of a modified Shockley-Read-Hall approach to take account of the double-occupancy and correlation energy between the D+/0

and D0/− transitions was applied [15,16]. No approximations limiting the transitions to capture processes as in [17] have been introduced. The correlation energy considered here was U_{corr} = 0.25 eV, similar to the a-Si:H structure [18]. Band tails were not included in the representation of the interface recombination-centre distribution. Capture coefficient values for the electron and hole capture into charged defects were: $c_n^{D+} = 1 \times 10^{-7}$ cm^3 s^{-1}, $c_n^{D0} = 1 \times 10^{-8}$ cm^3 s^{-1}, $c_p^{D-} = 1 \times 10^{-7}$ cm^3 s^{-1} and $c_p^{D0} = 1 \times 10^{-8}$ cm^3 s^{-1}, where the subscript denotes the carrier type and the superscript denotes the type of dangling bond into which the free carrier is captured. In the simulation, the a-Si:H/c-Si interface layer was represented by a 2 nm thin c-Si type defect layer with a chosen defect density, which is then translated to an interface defect density, N_{if}. Good agreement between experimental and simulation results is achieved with $N_{if} = 6.4 \times 10^{11}$ cm^{-3}, which is the value in the employed simulations. A similar value has been determined in [19] from surface photovoltage experiments on a-Si:H passivated c-Si wafer with HF pre-treatment before the a-Si:H deposition.

5. Results

5.1. Photoluminescence spectra of a-Si:H/c-Si heterostructures

For the analysis of the PL spectra of samples with different front and back reflection properties it is necessary to properly take into account the absorptivity term in order to track the different outcoupling properties for the photoluminescence emitted from these structures. The absorptivity according to Eq. (1) changes for the different layer sequences, especially after deposition of the metal back contact and the front TCO. Fig. 2 shows the calculated $A(\hbar\omega)$ for three different cases: a c-Si wafer, passivated with a-Si:H layers on both sides and with identical front and back reflection coefficients, the wafer with an additional Al back contact and the final device with a ZnO front contact. The reflection coefficients were assumed to be wavelength independent. The connection to the experimental value is based on the measured reflection in the high-energy range of Fig. 2. For the solely a-Si:H covered surfaces, we have determined R = 0.308 neglecting the effect of the thin amorphous silicon layers. In the shown spectral range of Fig. 2, R_F = 0.2 for the ZnO covered surface.

Figure 2 shows that at high photon energy $A(\hbar\omega)$ according to Eq. (1) saturates at $1 - R_F$. Here, the product of αd is much larger than 1 so that the exponential terms can be neglected and only 1- R_f remains in the expression for $A(\hbar\omega)$ in Eq. (1) [8]. At lower photon energies, re-absorption is less important so that the back reflection properties determine the output. As we consider the sample with the Al back contact having mirror properties and R_B = 1, $A(\hbar\omega)$ increases for energies $\hbar\omega$ < 1.25 eV,

compared with the symmetric structure. If the front reflection is less, as in the case of the ZnO layer, the output is even higher. It is noted that for the same quasi-Fermi level splitting, the measured PL intensity will be different solely due to the different absorptivity/emissivity spectra..

The front reflection of the structure also influences the photon flux that enters through the front interface. This variation must be taken into account when the PL spectra of Fig. 3 for the different structures are compared and discussed. Fig. 3 shows the spectral quantitative PL-yield measured from the different structures. The black dotted lines are analytically derived from Eq. (2). Adjustments of the analytical spectra yield an error of 4 meV for the deduced values of $E_{Fn} - E_{Fp}$. Full symbols show the results from asymmetric structures with differently doped layers and Al and ZnO additions. The open symbols represent measurements with the symmetrical structures.

For the symmetric structures there is a distinct increase in the quasi-Fermi level splitting of about 25 meV which will be discussed in more detail in the next section. For the processing steps of the solar cell denoted by the full symbols it can be seen that $E_{Fn} - E_{Fp}$ increases after each step. For the ZnO layer sample, the excitation photon flux is increased as the front reflection of the ZnO is 0.1 at the photon energy of the excitation laser, in contrast to the 0.3 for the a-Si:H front layer sequences. We can thus calculate the increase in the quasi-Fermi level splitting, which results from the increased excitation flux.

Translating this increment of the photon flux into the splitting of the quasi-Fermi levels, assuming that each absorbed photon generates one electron – hole pair, yields

$$\Delta(E_{Fn} - E_{Fp}) = kT \ln\left(\frac{\Phi_{\gamma,\mathrm{ZnO}}}{\Phi_{\gamma}}\right) = kT \ln\left(\frac{0.9\Phi_0}{0.7\Phi_0}\right) = 7\mathrm{meV},$$

where $\Phi_{\gamma,\mathrm{ZnO}}$ (Φ_{γ}) is the photon flux entering the silicon wafer with (without) the ZnO layer and Φ_0 is the photon flux impinging on the wafer. Fig. 3 shows that, in good agreement with these considerations, the experimental increase is 8 meV between the structure with and without the ZnO, i.e., the increase of the quasi-Fermi level splitting and of the PL output is solely due to the higher excitation level.

Figure 3 shows that the deposition of the Al layer leads to a further increase in PL yield over the whole spectrum. From the consideration for *A* from Fig. 2, we would expect an increase in the PL yield but we would not expect an increase in the high-energy range for photon energies > 1.25 eV if the quasi-Fermi level splitting remains unchanged. However, the experimental result for our structure is an

increase in $E_{Fn} - E_{Fp}$ of 6 meV from 661 meV to 667 meV after the Al deposition, which indicates an increased minority carrier density. We note, that despite the error of 4 meV for each value of $E_{Fn} - E_{Fp}$, the hierarchy in PL yield and the relative increase, respectively, from the different structures has always been maintained.

5.2. Simulation results for the symmetrical structures

The band diagrams of the two symmetric structures are depicted in Figs. 4(a) and 4(b). For the structure with the additional doped layer, i.e., the layer sequence (n)a-Si:H/(i)a-Si, the band bending is dominated by the doped n-type amorphous silicon because the intrinsic a-Si:H layer is very thin with a low charge density and its effect can be neglected. By comparison of both figures it can be seen that the occupancy and charge of the defects must change because the relative position of the interface Fermi level changes.

Figure 5 shows simulation results of the interface recombination rate R_{if} (Eq. (A1)) for the (i)a-Si:H/(p)c-Si/(i)a-Si:H and (n)a-Si:H/(i)a-Si:H/(p)c-Si/(i)a-Si:H/(n)a-Si:H structures when the peak position E_P of the defect distribution of width σ = 0.2 eV varies with respect to the valence band edge, ($E_P - E_V$). The values of R_{if} are higher for the structure with the additional n-layers, apart from the values at which E_P is close to the c-Si conduction band edge.

There is a strong anti-correlation between the interface recombination rate and the splitting of quasi-Fermi levels, taken here as an average value from the c-Si volume, as depicted in Fig. 6. As expected, high interface recombination results in a decrease in minority carrier density and thus reduces the quasi-Fermi level splitting in the volume of the wafer (and vice versa). For the passivation with (i)a-Si:H, $E_{Fn}-E_{Fp}$ reaches a minimum at mid-gap while adding (n)a-Si:H increases $E_{Fn}-E_{Fp}$ when defects are moved towards the conduction band.

From the experimental results of Fig. 3, a difference of (25 ± 8) meV between the splitting of quasi-Fermi levels $E_{Fn}-E_{Fp}$ is observed. A value of (600 ± 4) meV is measured when the wafer is passivated with (i)a-Si:H, which increases to (625 ± 4) meV with the addition of an (n)a-Si:H layer on both sides. Inspection of Fig. 6 shows that these experimental findings are met when $E_P - E_V$ lies in the range 0.7 to 0.8 eV.

To take account of the nature of the defects and their energetic distributions, Fig. 7 focuses on the energy range close to 0.7 eV and introduces some parameter variation. The open symbols are those of Fig. 6. The full symbols are from additional simulations with σ = 0.1 eV and slightly different sets of capture coefficients $c_n^{D+} = 8 \times 10^{-8}$ cm^3 s^{-1}, $c_n^{D0} = 4 \times 10^{-8}$ cm^3 s^{-1}, $c_p^{D-} = 4 \times 10^{-8}$ cm^3 s^{-1} and $c_p^{D0} = 8 \times 10^{-9}$ cm^3 s^{-1}, adopted by Froitzheim in the simulation part of his work [19]. The full symbols show a similar variation in $E_{Fn}-E_{Fp}$ with a slightly larger $E_{Fn}-E_{Fp}$ difference between the two structures. The circle in Fig. 7 indicates the range of $E_P - E_V$ for which a variation in the parameters leads to the

experimentally determined difference in $E_{Fn}-E_{Fp}$ of about 25 meV.

5.3. Complementary results for asymmetrical structures

Figure 8 summarises experimental and simulation results for the quasi-Fermi leve splitting in the symmetric structures, where the range of experimental data points results from measurements at different positions on the sample. The asymmetric structure with a "back surface field" layer (structure c of Fig. 1) shows a further increase in $E_{Fn}-E_{Fp}$. The simulation results, determined with the same parameter set, reproduce the correct trends.

In order to substantiate the agreement between the simulated and the experimental results, we have also measured electrically the open-circuit voltage of the solar cell (structure d of Fig. 1) under AM1.5 illumination, and obtain a value of 590 mV. Simulation of the solar cell with identical parameters to those used in the wafer modelling results in V_{OC} = 591 mV, under the same AM1.5 illumination conditions.

6. Discussion

Our analysis takes into account the different aspects of the variations in the coupling of light into and out of the wafer structures, and we have adjusted the analytical spectra with different $A(\hbar\omega)$ to obtain a correct description of the absorptivity/emissivity, as shown in Fig. 3. This gives an insight into why changes in the quasi-Fermi levels occur after different processing steps, notably after the ZnO and Al deposition. When the ZnO layer is added, there is an increase in the excitation and emission flux due to variations in the reflectivity and absorptivity of the wafer which causes a higher quasi-Fermi level splitting. However, the analysis has shown that this increase is solely attributed to the higher excitation flux after ZnO deposition and not to any intrinsic changes in internal field.

Similarly, reflection of PL radiation at the Al back contact increases the PL flux, which is coupled out. Because of re-absorption, there is no additional flux in the high energy range of the PL spectrum in which $E_{Fn} - E_{Fp}$ is usually determined. This has been demonstrated by placing a separate mirror at the back side of a symmetric structure [14]. Thus, after Al deposition, no increase in $E_{Fn} - E_{Fp}$ is expected. However, a higher $E_{Fn} - E_{Fp}$ has been detected for the structure with the Al back contact. This can be accounted for by a small increase in the doping level at the back interface by diffusion of Al into the (p)a-Si:H layer, and consequent enhancement of the passivation quality at the back of the wafer. Further systematic investigations (e.g. by SIMS profiling) will be needed to fully understand this effect.

Concerning the symmetric structures in Fig. 3, the quantitative PL yields an increased output when comparing the (i)a-Si:H/(p)c-Si/(i)a-Si:H and (n)a-Si:H/(i)a-Si:H/(p)c-Si/(i)a-Si:H/(n)a-Si:H structures.

The appeal of this comparison is that the (i)a-Si:H/(p)c-Si interface defect distribution is the same in both structures. The only difference would be the changed occupancies under illumination which are influenced by the highly-doped (n)-a-Si:H layer, and are included in the numerical solutions for the whole system.

The simulation results have shown that there is a variation in the quasi-Fermi level splittings of the two structures when the simulation parameters are varied slightly. This is observed e.g. for different widths of the distribution in Fig. 7. The simulations show also that a flat distribution, with Gaussian width > 0.5 eV, does not predict the experimental result but in fact to the opposite effect, with a higher PL yield for the (i)a-Si:H structure. For very narrow distributions with width < 0.01 eV the difference in quasi-Fermi level splitting increases to much higher values than observed experimentally.

It is not the aim of the simulation study to track in detail all the features of the experimental results. Given the scatter in the experimental values, which depend on the different measurement positions on the sample, and the range of plausible simulation parameter values one can say that the experimental trend is very well reproduced, especially since the simulation results agree with the experimental trend across the three different structures in Fig. 8. Also, the good agreement in the open-circuit voltage between the experimental and simulated solar cell (d of Fig. 1) adds confidence in the conclusion that, within the model we have used, the interface defect peak lies in the range 0.7 eV – 0.8 eV above the c-Si valence band edge, with a Gaussian width around 0.1 eV.

7. Conclusions

An advantage of photoluminescence measurements, as a contactless method, is to enable the analysis of consecutively processed layers during device deposition, and thereby the evaluation of each of the process steps. By taking into account the different contributions to the PL yield, from the excitation flux to the two terms in Planck's generalised law – quasi-Fermi level splitting and absorptivity – we have distinguished between cases in which a higher PL flux is related to a larger quasi-Fermi level splitting, i.e., minority carrier density, and those where other factors are involved. While the higher PL yield after ZnO deposition is solely related to a higher excitation flux, the deposition of Al was shown to result in a higher quasi-Fermi level splitting with improved back-interface properties.

From the differences in relative and absolute terms in the PL yield of the symmetric (i)a-Si:H/(p)c-Si/(i)a-Si:H and (n)a-Si:H/(i)a-Si:H/(p)c-Si/(i)a-Si:H/(p)a-Si:H structures with the same (i)a-Si:H/(p)c-Si interface properties, we deduce the energetic position of the interface defect distribution. Although the energetic value is not unambiguous, simulations using a range of plausible parameter sets indicate a position of 0.7 to 0.8 eV above the c-Si valence band edge and a Gaussian width in the range of 0.1

eV. The analysis is supported by electrical measurements of the solar cell open-circuit voltage, which could also be reproduced with the same simulation parameter set.

Acknowledgements

The authors thank G.H. Bauer for valuable discussions and suggestions. They also thank their colleagues at IPE, Stuttgart, for sample preparation and M. Scherff at FernUniversität Hagen for complementary measurements. Financial support by BMBF contract 01SF0115 and EWE Stiftung is gratefully acknowledged.

Appendix

The statistics of the interface defects is taken to follow the well-established statistics developed for dangling bonds in a-Si:H which takes into account the three charge states positive, neutral and negative [15,16]. Thus, the defect density at an energy (E) is the sum of the densities in the different charge states $D^+(E)$, $D^0(E)$ and $D^-(E)$. The electron interface-defect recombination rate R_{if} is given by the net loss via two paths as illustrated in Fig. A1. Taking into account the capture and emission rates, R_{if} reads

$$R_{if} = \int \left[(C_n^+ D^+ n - e_n^0 D^0) + (C_n^0 D^0 n - e_n^- D^-) \right] \mathrm{d}E \,, \qquad \text{(A1)}$$

with an integration over the energetic distribution and where the first brackets denote the $D^{+/0}$ transition (path I: $e + D^+ \leftrightarrow D^0$) and the second brackets the $D^{0/-}$ transition (path II: $e + D^0 \leftrightarrow D^-$), which are separated in energy by a correlation energy U [15,16]. Here, C_n^+ and C_n^0 are the capture coefficients for electron capture into positive and neutral interface defects and e_n^0 and e_n^- describe the effective electron emission rates from the neutral and negative interface defect into the conduction band. A closed-form expression for R_{if} in Eq. (A1) in terms of the free electron (n) and free hole (p) densities can be derived [15,16].

References

[1] G. Sasaki, S. Fujita and A. Sasaki 1982 *J. Appl. Phys.* **53** (2) 1014-17.

[2] M. Tanaka, M. Taguchi, T. Matsuyama, T. Sawada, S. Tsuda, S. Nakano, H. Hanafusa and Y. Kuwano 1992 *Japan. J. Appl. Phys.* **31** (11) 3518-22.

[3] F. Roca, G. Sinno, G. Di Franca, P. Prosini, G. Fameli, P. Grillo, A. Citarella, F. Pascarella and D. della Sala 1997 *Solar Energy Materials & Solar Cells* **48** (15) 1-4.

[4] M.L.D. Scherff, A. Froitzheim, A. Ulyashin, M. Schmidt, W. R. Fahrner and W. Fuhs 2002 PV in Europe 216-219.

[5] A. Froitzheim, M.L.D. Scherff, A. Ulyashin, O. Milch, M. Schmidt, W. R. Fahrner and W. Fuhs 2003 3rd World Conference in Photovoltaic Energy Conversion, 3. Vol. **A**. 180-183.

[6] K. von Maydell, M. Schmidt, L. Korte, A. Laades, E. Conrad, R. Stangl, M. Scherff and W. Fuhs 2005 31st Photovoltaic Specialists Conference, 1225-28.

[7] S. Tardon, M. Rösch, R. Brüggemann, T. Unold and G. H. Bauer 2004 *J. Non-Cryst. Solids* **444** 338-340.

[8] P. Würfel 1982 *J. Phys.* C **15** 3967-85.

[9] P. Würfel Physik der Solarzellen 2000 Spektrum Akademischer Verlag, Heidelberg

[10] T. Unold, D. Berkhahn, B. Dimmler and G.H. Bauer 2000 Proceedings 16th European Photovoltaic Solar Energy Conference 736-39.

[11] M. Rösch, R. Brüggemann and G.H. Bauer 1998 Proceedings of the 2nd World Conference on Photovoltaic Solar Energy Conversion 946.

[12] M. Rösch 2003 PhD thesis, Carl von Ossietzky Universität Oldenburg, online at docserver.bis.uni-oldenburg.de/publikationen/dissertation/2003/roeexp03/pdf/roeexp03.pdf

[13] T.Unold, M. Rösch and G.H. Bauer 2000 J. non-Cryst. Solids **266** 1033-1037, Part B

[14] R. Brüggemann, J. Behrends, S. Meier, S. Tardon 2007 J. Optoelectr. Adv. Mater. **9** 77-83.

[15] H. Okamoto, H. Kida and Y. Hamakawa 1984 Philos. Mag. B **49** 231.

[16] C. Main, J. Berkin and A. Merazga, in New Physical Problems in Electronic Materials, edited by M. Borissov, N. Kirov, J. M. Marshall, and A. Vavrek, (World Scientific Press, Singapore, 1991) p. 55.

[17] S. Olibet, E. Vallat-Sauvain, and C. Ballif 2007 Phys. Rev. B **76** 035326.

[18] R. A. Street Hydrogenated Amorphous Silicon 1991 Cambridge University Press, Cambridge.

[19] A. Froitzheim 2003 PhD thesis Philipps-Universität Marburg.

FIGURE CAPTIONS

Figure 1: Illustration of the samples investigated: a) c-Si absorber passivated symmetrically with two 8 nm thin (i)a-Si:H layers, b) the structure of a) with additional two 8 nm (n)a-Si:H layers, c) asymmetric (n)a-Si:H/(i)a-Si:H/(p)c-Si/(i)a-Si:H/(p)a-Si:H and d) (n)a-Si:H/(p)c-Si solar cell with symmetric 8 nm (i)a-Si:H buffer layers and a 20 nm (p)a-Si:H "back surface field" layer and an Al back contact.

Figure 2: Calculated absorptivity of the (p)c-Si wafer for different reflection coefficients at the front and back. For the samples according to Fig. 1 (a-c), the same reflectivity at the front and back of the wafer has been assumed ($R_F = R_B = 0.308$) (dotted line). The addition of a ZnO layer reduces the reflection at the front in the spectral range shown ($R_F = 0.2$), which results in an increase of A at higher energies from 0.692 to 0.8 (dashed line). The addition of a back contact as in Fig. 1(d) produces a reflector ($R_B = 1$) and A increases for energies $\hbar\omega < 1.25$ eV (full line).

Figure 3: Quantitative photoluminescence after different steps of c-Si wafer and a-Si:H/c-Si solar cell processing (full symbols) and of symmetric structures (open symbols) with the corresponding quasi-Fermi level splitting. The dotted lines are calculated with the analytical expression of Kirchhoff´s generalised law (Eq. 2).

Figure 4: Calculated band diagram in thermodynamic equilibrium of the 2 symmetric structures of Fig. 1. In the diagram, the energetic distribution of defects at the interface is shown schematically.

Figure 5: Total interface recombination rate versus energetic position of the defect peak relative to the valence band edge.

Figure 6: Corresponding splitting of quasi-Fermi levels for different energetic positions of the defect peak at the interface for the (i)a-Si:H (squares) and (n)a-Si:H/(i)a-Si:H (circles) passivated wafers. The simulation has been performed for two different parameter inputs: $\sigma = 0.2$ eV and (open squares and circles) and $\sigma = 0.1$ eV (crossed squares and circles). The capture coefficients were also different (see text). The experimental results can be reproduced in the numerical calculation by an energy peak around 0.7 eV for interface defects

Figure 7: Splitting of quasi-Fermi levels for different energetic positions of the defect peak. The simulation has been done for different parameter input: $\sigma = 0.2$ eV (open squares and circles) and $\sigma = 0.1$ eV (full squares and circles). The capture coefficients were slightly different (see text). The shaded

areas indicate the ranges of the ordinate scale for the experimental results of the two types of structures. They can be reproduced in the numerical calculations by an energy peak around 0.7 – 0.8 eV for the interface defects

Figure 8: Splitting of the quasi-Fermi levels obtained from quantitative photoluminescence measurements and simulated for the symmetric structures a), b) and c) of Fig. 1. In a good correlation between the experiments and the simulation, the $E_{Fn} - E_{Fp}$ values increase correspondingly.

Figure A1: Transition diagram for the recombination via dangling bonds showing the possible transitions of electrons and holes for the three charge conditions. Emission is denoted by dashed arrows, free-carrier capture by full arrows.

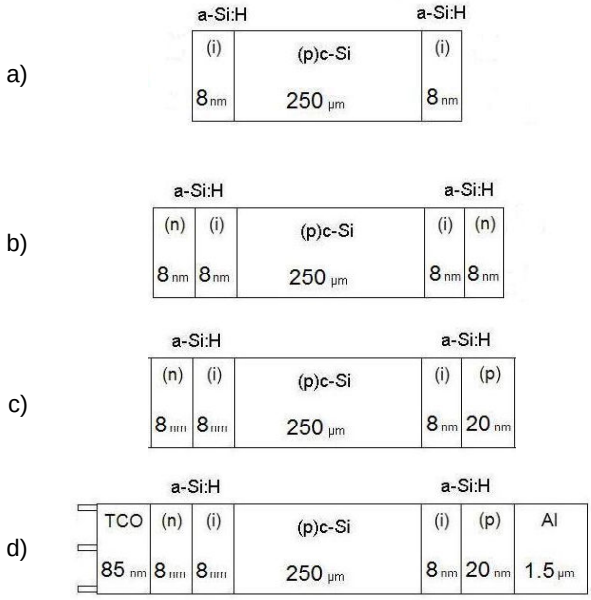
a)
a-Si:H
a-Si:H
(i)
8 nm
(p)c-Si
250 µm
(i)
8 nm
b)
a-Si:H
a-Si:H
(n)
8 nm
(i)
8 nm
(p)c-Si
250 µm
(i)
8 nm
(n)
8 nm
c)
a-Si:H
a-Si:H
(n)
8 nm
(i)
8 nm
(p)c-Si
250 µm
(i)
8 nm
(p)
20 nm
d)
a-Si:H
a-Si:H
TCO
85 nm
(n)
8 nm
(i)
8 nm
(p)c-Si
250 µm
(i)
8 nm
(p)
20 nm
Al
1.5 µm

Figure 1

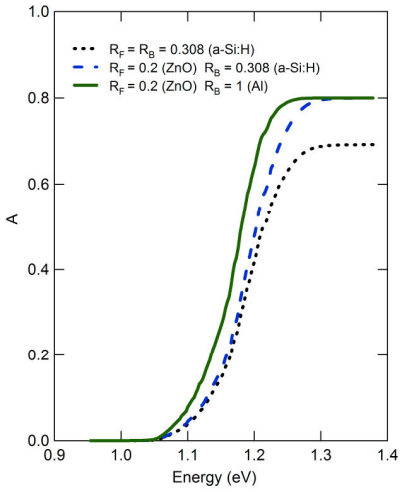
$R_F = R_B = 0.308$ (a-Si:H)
$R_F = 0.2$ (ZnO) $R_B = 0.308$ (a-Si:H)
$R_F = 0.2$ (ZnO) $R_B = 1$ (Al)
A
Energy (eV)
1.0
0.8
0.6
0.4
0.2
0.0
0.9
1.0
1.1
1.2
1.3
1.4

Figure 2

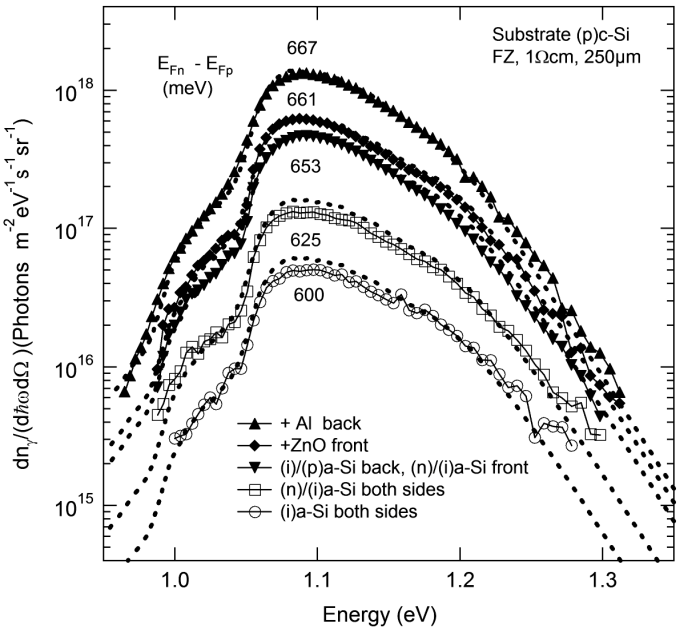
Substrate (p)c-Si
FZ, 1Ωcm, 250μm
E_{Fn} - E_{Fp}
(meV)
667
661
653
625
600
+ Al back
+ZnO front
(i)/(p)a-Si back, (n)/(i)a-Si front
(n)/(i)a-Si both sides
(i)a-Si both sides
$dn_\gamma/(d\hbar\omega d\Omega)$ (Photons $m^{-2} eV^{-1} s^{-1} sr^{-1}$)
10^{18}
10^{17}
10^{16}
10^{15}
1.0
1.1
1.2
1.3
Energy (eV)

Figure 3

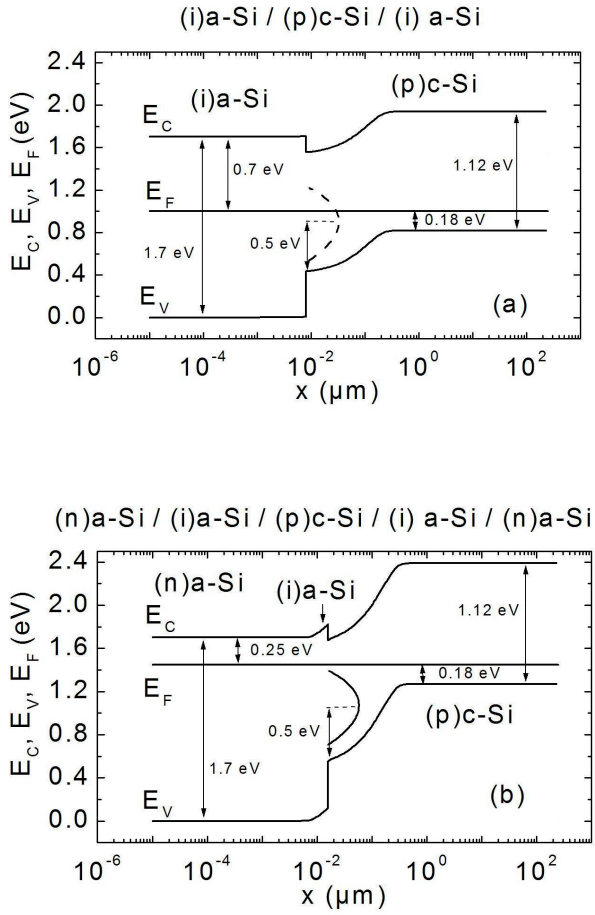
(i)a-Si / (p)c-Si / (i) a-Si
(i)a-Si
(p)c-Si
E_C
E_F
E_V
0.7 eV
1.12 eV
0.18 eV
0.5 eV
1.7 eV
(a)
E_C, E_V, E_F (eV)
x (μm)
(n)a-Si / (i)a-Si / (p)c-Si / (i) a-Si / (n)a-Si
(n)a-Si
(i)a-Si
(p)c-Si
0.25 eV
1.12 eV
0.18 eV
0.5 eV
1.7 eV
(b)

Figure 4

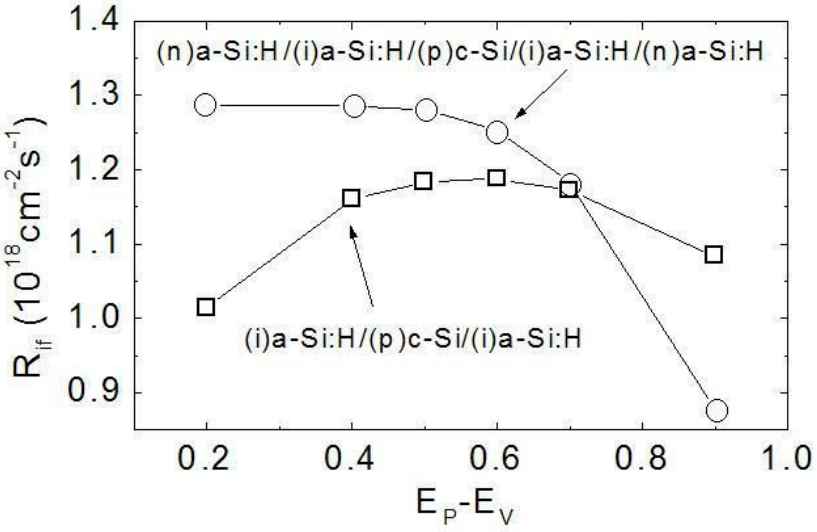
(n)a-Si:H/(i)a-Si:H/(p)c-Si/(i)a-Si:H/(n)a-Si:H
(i)a-Si:H/(p)c-Si/(i)a-Si:H
R_{if} ($10^{18}cm^{-2}s^{-1}$)
E_P-E_V
1.4
1.3
1.2
1.1
1.0
0.9
0.2
0.4
0.6
0.8
1.0

Figure 5

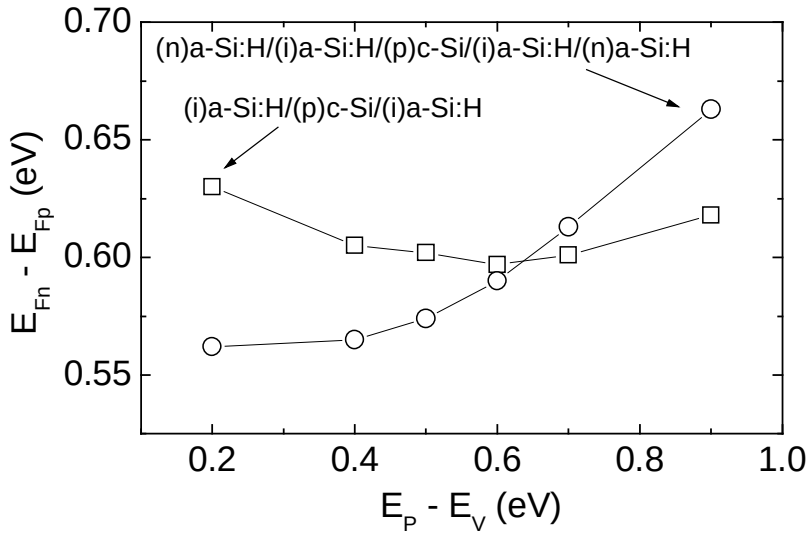
(n)a-Si:H/(i)a-Si:H/(p)c-Si/(i)a-Si:H/(n)a-Si:H
(i)a-Si:H/(p)c-Si/(i)a-Si:H
0.70
0.65
0.60
0.55
0.2
0.4
0.6
0.8
1.0
E_Fn - E_Fp (eV)
E_P - E_V (eV)

Figure 6

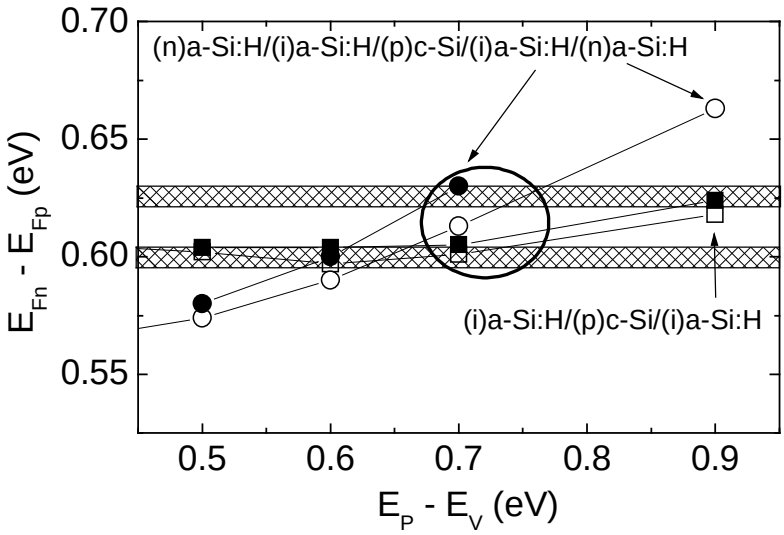
(n)a-Si:H/(i)a-Si:H/(p)c-Si/(i)a-Si:H/(n)a-Si:H
(i)a-Si:H/(p)c-Si/(i)a-Si:H
0.70
0.65
0.60
0.55
0.5
0.6
0.7
0.8
0.9
E_Fn - E_Fp (eV)
E_P - E_V (eV)

Figure 7

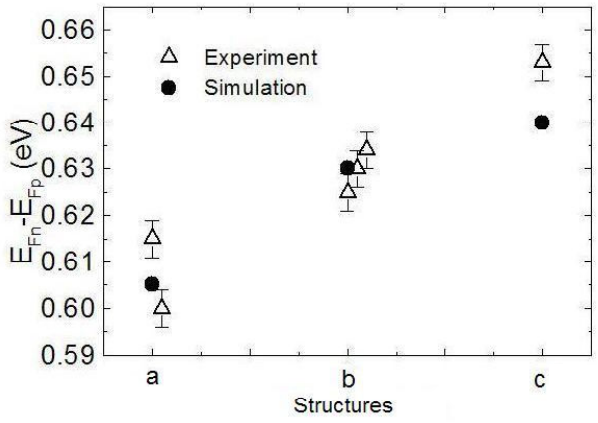
0.66
0.65
0.64
0.63
0.62
0.61
0.60
0.59
E_{Fn}-E_{Fp} (eV)
Experiment
Simulation
a
b
c
Structures

Figure 8

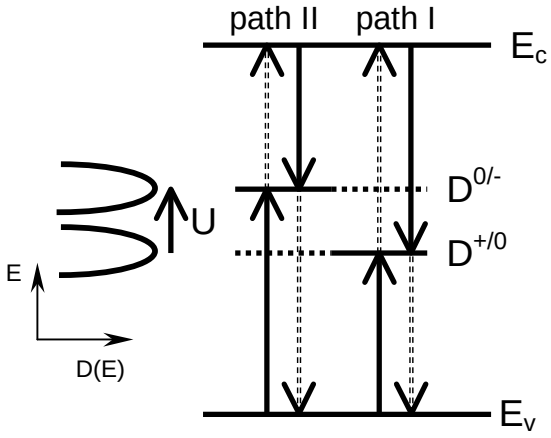

Figure A1